Pulsed Laser Induced Nanoparticle Formation on Stainless Steel for Carbon Nanotube Growth

Aiden Zurcher

NanoProduct Lab

Dr. Mostafa Bedewy

April 28th, 2026

Abstract

Carbon nanotubes (CNTs) can provide a multitude of different advantages when they are grown directly on stainless steel (SS). This is possible using chemical vapor deposition (CVD). However, a pre-synthesis annealing step in air is required before the CVD process. This step is slow, high energy and imprecise. Instead of annealing, this study examined the viability of using a green pulsed (532 nm wavelength) laser on 2-inch disks of 304 SS to grow different thicknesses of oxide layers. This approach has been reported before only by Dasbach et al. They used the term dewetting cycles, or DCs, a conflation of laser frequency and scanning speed, as their independent variable. They assumed that surface dewetting was dominate process in the creation of nanoparticles on SS. The hypothesis of this study was that laser frequency and scanning speed have differing effects on the SS surface, and therefore VA-CNT growth. Agglomeration and diffusion of iron and nickel across the chromium-rich oxide layer was expected to be the dominating cause of nanoparticle formation, not dewetting. The results from the laser power tests, examination of the SS surface coloration, SEM, and SEM-EDS largely support this hypothesis. There are still significant gaps left by the research, that require further study in this unique field.

Introduction

Carbon nanotube (CNT) forests, or vertically aligned carbon nanotubes (VA-CNTs) are one morphology of carbon nanotubes with unique properties and applications. VA-CNTs consist of many CNTs grown perpendicularly from a substrate. They ideally differ from CNT networks by being straight and aligned in this manner, though van der Waals forces cause them to interact and tangle.

The electrical properties of VA-CNTs enable their use as current collectors in lithium-ion batteries [1] and conductive electrodes in perovskite solar cells [2]. Especially when grown on metal substrates, the hydrophobicity, compressive strength, and recoverability of VA-CNTs enable their use as coatings [3]. Additionally, VA-CNTs are effective at thermal management between interfaces [4]. These properties are correlated with the structure and alignment of the VA-CNTs.

The most frequently used method of manufacture for VA-CNTs is Chemical Vapor Deposition (CVD) [5]. Compared to alternatives such as laser ablation and arc discharge, CVD is far more scalable, cheaper, and has a higher yield. For these reasons, CVD is the industry standard. This process involves heating metal nanoparticle catalysts: typically nickel, cobalt and iron, to about 700˚C. Then, two gasses are added into the reactor chamber. One gas is hydrocarbon and the other maintains the pressure. At high temperatures, the hydrocarbon gas is split, and dissolves into the catalyst. The diameter of the CNTs that grow from the catalyst depends upon the size of the nanoparticle catalysts.

In laboratory environments, VA-CNTs are typically grown from nanoparticles on top of a substrate such as silicon. These nanoparticles are either deposited on the surface or arise through dewetting a thin metallic film. In this study, VA-CNTs were grown on samples of 304 stainless steel (SS). This is possible because SS contains metals that seed CNT growth within its composition. These catalysts take the form of pure iron, Fe–Cr, and Fe–Ni nanoparticles [6]. In addition to increasing accessibility and the attachment strength by growing the VA-CNTs on to the SS without an adhesive, it has been shown that SS functions as an effective substrate. SS can be used to create complex geometries such as meshes, foils, and fibrous structures, that cannot be easily replicated by other substrates [3]. Another advantage to growing VA-CNT directly from SS is the increased bond strength between the two materials.

Thermal oxidation is the most used method to produce nanoparticles on the surface of stainless steel. This process is slow and difficult to precisely control. In this study, pulsed lasers were examined as alternative method to induce nanoparticle formations. This was only performed before by a group in Germany, Dasbach et al. [8], who found that lasers enabled precise control of the VA-CNT morphology. They attributed the process of nanoparticle formation to rapid dewetting of the surface of the stainless steel. Through this, they predicted that the surface layer rapidly transforms from a liquid phase and back as the laser pulses many times. They used the term “dewetting cycles” or DCs to keep track of the number of times that a given location is hit by a laser. Dasbach et al found that nanoparticle density and therefore VA-CNT length were maximized

within a certain range of DCs. The approximate formula for DCs is listed in Equation 1, where d is the laser diameter, v is the laser scanning speed, and f is the laser frequency.

$$DC = \frac{d}{v} f \quad [1]$$

DCs as a concept are a simplification of the interaction behavior between lasers and SS. It is the objective of this study to decouple frequency and scanning speed from each other for the purpose of explaining their effects on the resulting growth patterns of VA-CNTs on SS. Furthermore, it is hypothesized that dewetting cycles is a misnomer, as the main force for producing surface nanoparticles is not the rapid liquification of the SS surface, but instead agglomeration of iron-nickel nanoparticles through diffusion across the chromium oxide layer.

Splitting frequency and scanning speed in this manner is necessary because they both have different effects on the surface structure of the SS. Scanning speed has a dominant effect on the fluence, the total energy delivered per area. This was predicted to be a knob that can control the size of grooves and craters on the surface, even to the point of cutting at low scanning speeds. Decreasing scanning speed is expected to increase the feature density. Frequency, on the other hand, has a dominant effect on the pulse energy. Higher frequencies were predicted to have a stronger effect on increasing heat accumulation and thickening surface oxidations layers. These relations can be seen from the formula of pulse energy used for calculation in Equation 2, and the formula for fluence in Equation 3. In these equations, E_p is pulse energy, P is power, f is frequency, F is fluence, N_{eff} is the number of overlapping pulses (derived from scanning speed), and A is the area of the laser.

$$E_p = \frac{P}{f} \quad [2]$$

$$F = \frac{N_{eff} E_P}{A} \quad [3]$$

Controlled oxidation of the SS surface after polishing completely smooth is expected to introduce nanoscale roughness. The presence of chromium in the oxide layer of the stainless steel inhibits the diffusion of the iron nanoparticles back into the bulk. Increasing the oxide layer through higher frequencies will lead to an increase in carbon nanotube diameter due to additional iron atoms diffusing through the chromium-rich layer, increasing the size of the nanoparticle catalysts [9]. Too much oxidation, indicated by too high frequency or too many DCs has a deleterious effect on the quality of VA-CNTs, however [8].

Precisely managing the iron content of the catalyst nanoparticles is important for VA-CNT growth [6]. This is a function that can be effectively carried out by a pulsed laser. The pulsed laser process has the simultaneous effect of changing the composition ratio of the oxide layer away from silicon oxide and toward iron and chromium – ideal metals for the growth of VA-CNTs. This is due to the difference in oxide affinity in each element and therefore followed the pattern of Si >

Mn > Cr > Fe > Ni, with increasing DCs [10]. This gave the result that about 100 DCs were the ideal amount for catalyst density and CNT height on 304 SS. This number is difficult to replicate due to the combination of different variables, giving an added benefit to decoupling them.

Experimental Procedure

16 2-inch diameter, 1 mm thick disks of 304 stainless steel were acquired for testing. The laser was Keyence's Telecentric Laser Marker in the MD-T Series. This model is a Q-switch 532 nm wavelength laser. It has a frequency range of 1-400 kHz. The maximum scanning speed was 12000 mm/s, but no scanning speed higher than 1000 mm/s was tested. The laser was focused to a distance of 6cm from the plane, creating a laser diameter of 30 micrometers. The software used was Marking Builder 2 with the DXF add-on. Hatch designs were created horizontally with 3 micrometer hatch distance. Tests 1-5 were conducted on scrap pieces of stainless steel to calibrate the laser to the proper focus distance and general parameter scope. Each test consisted of an array of 5mm-by-5mm squares. About 42 squares could fit on one disk at a time.

Tests were conducted first to collect data on the precise power output of the laser at different frequencies and scanning speeds. The laser was held to 80% power, though the actual value depended heavily on the laser frequency. This data was plotted and then used to calculate the expected fluence and pulse energy.

Once the laser was setup and its power was determined, the tests on the SS disks began. Each disk was cleaned first with acetone, then with isopropyl alcohol to remove surface debris that was potentially acquired when they were machined. The specific sample parameters of each of the tests can be seen in Figure 1. Test 6 established a wide boundary of the parameter space, across the entire frequency range, and from 20 mm/s to 120mm/s scanning speed. Tests 6 and 13 held scanning speed constant, while test 11 held frequency constant. Tests 9, 12, 14, and 15 were conducted to explore the range established by test 6 in more detail. Tests 8 and 10 were made to examine the area with prismatic coloration attributed to thin film interference in more detail. Test 16 was made to examine the higher frequency area that had limited coloration because of its low fluence.

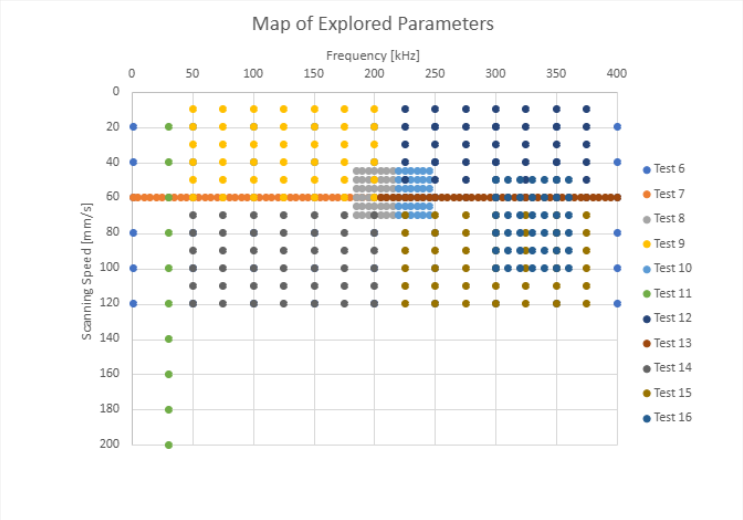

Figure 1

Map of tested combinations of frequency and scanning speed.

After these SS samples were processed with a laser, notable ones were put through the rapid thermal chemical vapor deposition reactor. This was a horizontal glass furnace with a 35 mm inner diameter and a 150 mm heating zone at 750 °C with a heating rate of 16 °C min−1. The carrier gas was helium, and the precursor was ethylene gas. Characterization techniques involved optical and SEM microscopy. SEM-EDS was also performed to further identify the atomic make-up of the post-CVD surface of the sample.

Results

As described in the experimental methods, the process began with testing the specifications of the pulsed laser. Figure 2 describes how the power varies with the frequency setting. It should be noted that despite remaining at 80% power, there is notable variance. The rapid drop in power at low frequencies was reflected in early tests, so from this point on, no lower than 25kHz was tested.

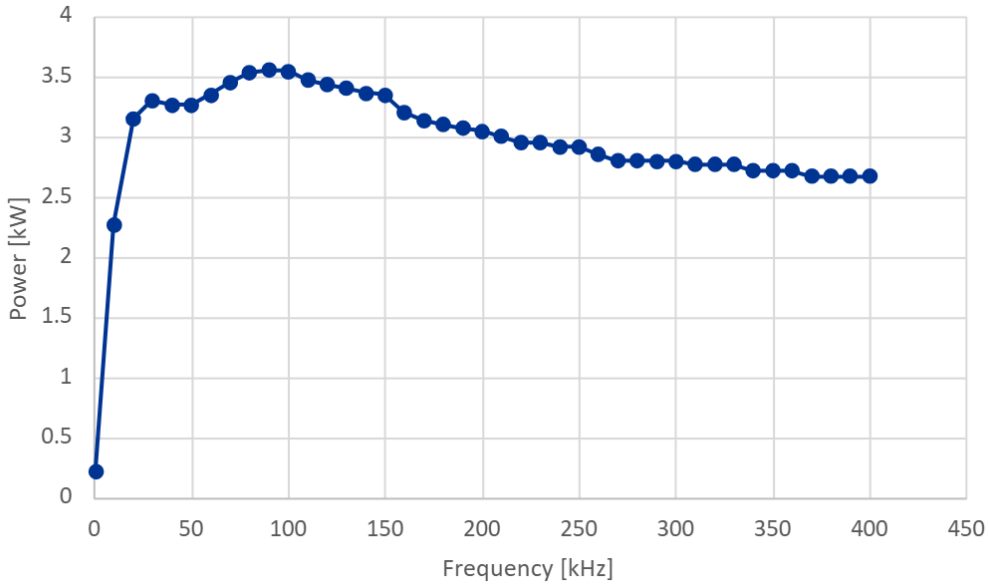

Figure 2.

Variation of Power with Frequency of Pulsed Laser set to 80% power.

Next, using Equation 2, frequency was graphed in Figure 3 in relation to the pulse energy. Scanning speed definitionally has no effect on pulse energy, so this is a knob controlled entirely by frequency. Due to the inverse relation between the two values, a small increase from a low frequency has a significant effect on the pulse energy. If the hypothesis is correct, it should be expected that the oxide layer variation on the resulting steel sample has the largest changes at low frequencies.

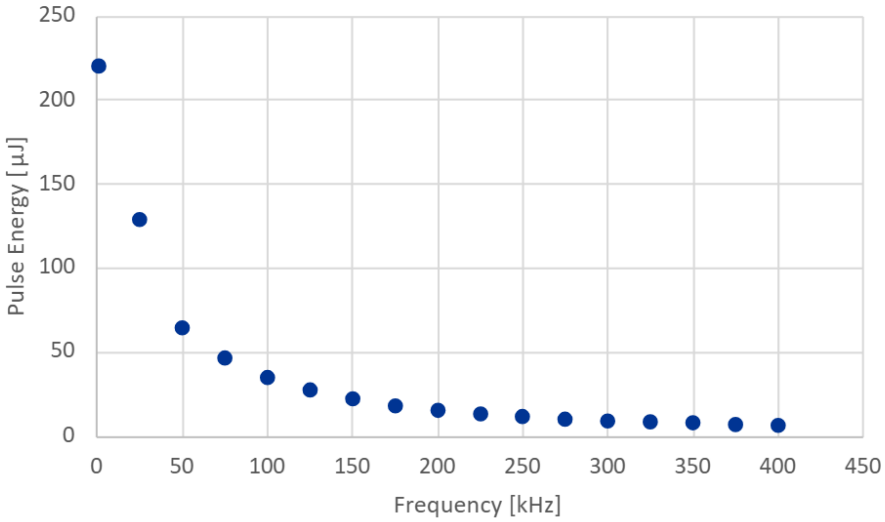

Figure 3

Relation of frequency and pulse energy using Equation 2.

Using Equation 3, fluence was graphed as a factor of both frequency and speed in Figure 4. Ignoring the massive drop off in fluence that arises from the drop off in power at very low frequencies, scanning speed has a clear dominant effect on fluence. Across the entire available frequency range of the q-switch pulse laser, fluence only changes by at most 200 J/cm^2, whereas scanning speed can change fluence from 800 J/cm^2, in the range of 40 mm/s.

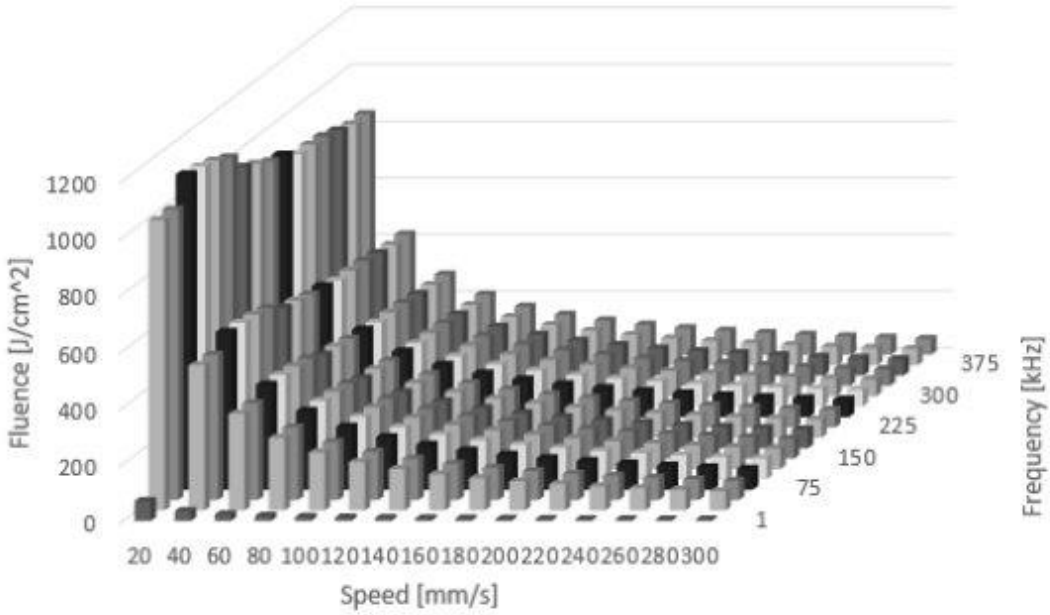

Figure 4

3D chart of the Effect of Frequency and Scanning Speed on the Laser Fluence at 80% Power.

After the laser process is completed, the colors of the result SS surface were documented in Figure 5. It should be noted that the actual color depends heavily on the incident light level, making documenting difficult and imprecise. Overall, the colors appear more muted in this document than they do physically. The tan shade in the high frequency and scanning speed region is not the real color of the surface. This area did not receive enough pulse energy to cause significant change in the size of the surface oxide layer and is very lightly shaded, almost identical to the color of the control surface. The tan color originates from the reflection of the white background. Around 200 kHz and 60 mm/s, thin film interference results in a prismatic coloration that wildly changes in color depending on viewing angle. This effect occurs in line with the horizontal hatch lines. Only rotating the sample around the constant scanning speed axis will demonstrate this effect. No color change occurs when rotating the sample around a constant frequency axis.

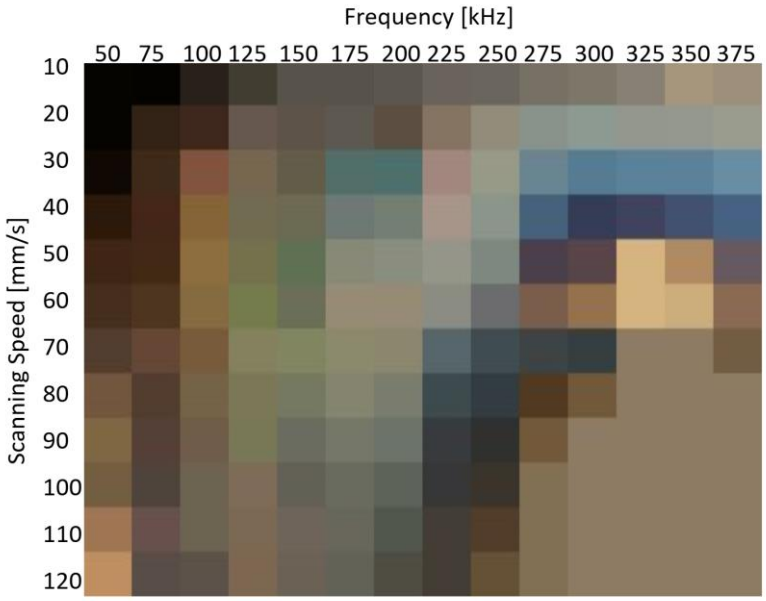

Figure 5.

Chart of the coloration of the SS surface based on scanning speed and frequency.

The images in Figure 6 show the 2-inch stainless steel disks with the coloration resulting from the laser before and after they entered the RT-CVD reactor. The small oxide layer section and the prismatic section are both visible on the initial sample. Additional amorphous carbon was

produced surrounding the disk that was ignored for the purposes of this study. The high temperatures thermally oxidized the rest of the stainless steel, but the carbon nanotubes only grew on the sections that had been prepared with the laser.

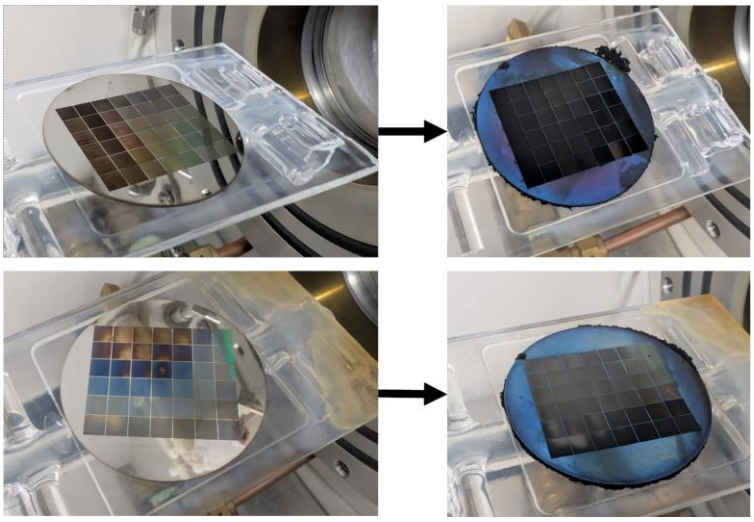

Figure 6

Before and after images of SS samples in the RT-CVD reactor

The following figures all show SEM results at different locations across the samples. Figure 7 is taken from the 50 kHz and 10 mm/s area of the sample. This is the location with the largest amount of fluence and pulse energy. The result is a cauliflower-like structure. This surface is completely destroyed. This is well documented in Dasbach et al.

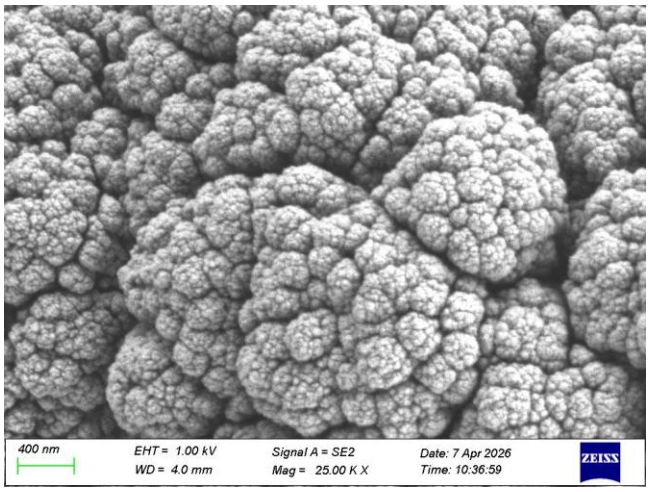

Figure 7.

SEM results showing a cauliflower structure of 50 kHz 10 mm/s square at 25k magnification.

The next figure is taken at the same location after the sample underwent CVD. CNTs are present, but their structure is not uniform and completely uncontrolled. This also matches the result documented by Dasbach et al.

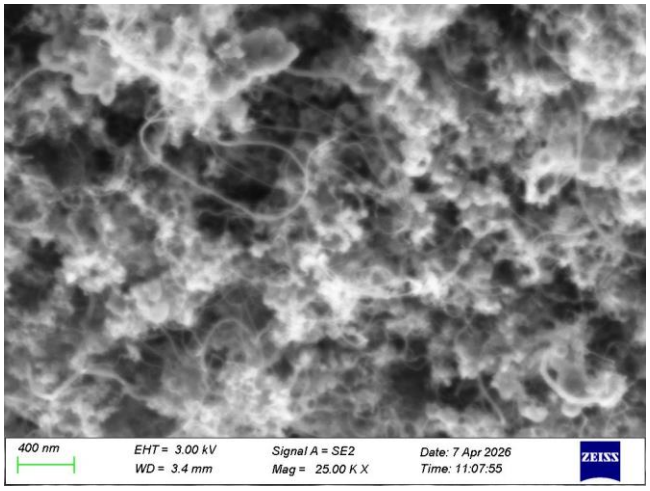

Figure 8.

SEM Results showing a post-CVD structure of 50 kHz 10mm/s square at 25k magnification.

This figure shows the extent of destruction of the same high fluence region on the pre-CVD sample. The laser has carved deep paths across the sample, because of its high fluence. It is taken at a much lower magnification.

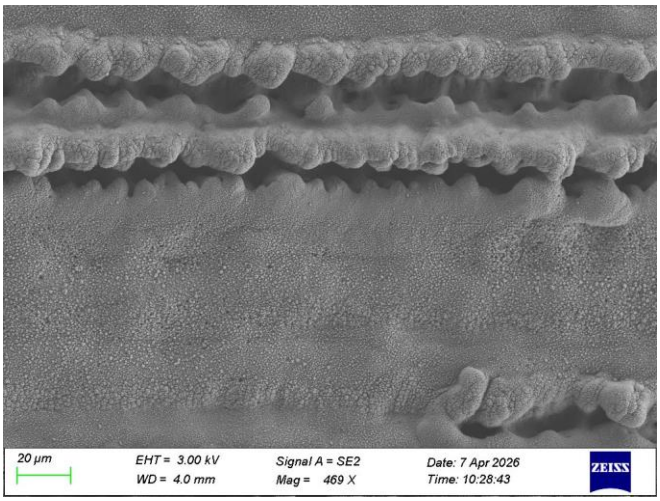

Figure 9.

SEM Results showing a pre-CVD structure of 50 kHz 10mm/s square at 469 times magnification. Clear carved canyons are present.

The following figure, figure 10, is taken at 175 kHz and 60 mm/s. It shows a surface free of the cauliflower structures, instead populated by numerous nanoparticles.

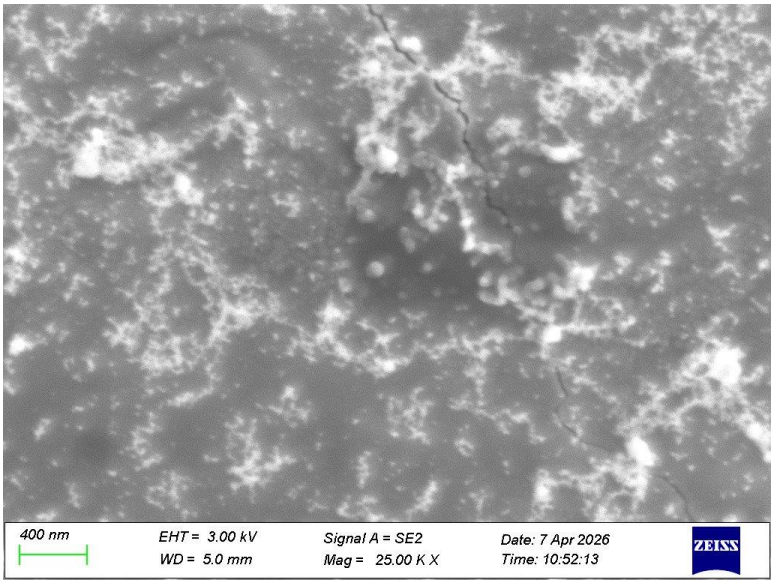

Figure 10

SEM results showing pre-CVD structure of 175 kHz 60mm/s square at 25k times magnification. Nanoparticle phases are present.

The last SEM image, shown in Figure 11, highlights a part of the same region as Figure 10, that exhibits good carbon nanotube growth. A less intensive magnification is used which enables more of the structure to become visible.

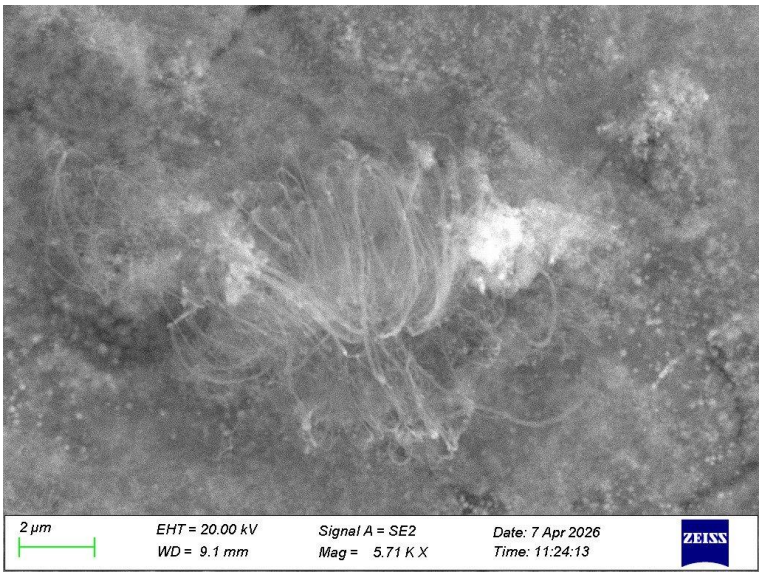

Figure 11

SEM results showing post-CVD structure of 175 kHz 60 mm/s square at 5.71k times magnification.

Figure 12 consists of three images collected after performing SEM-EDS on the area in figure 11. This process confirms the presence of carbon nanotubes due to the massive spike in carbon around the central nanotube's location. It also supports the hypothesis that carbon nanotubes growth occurs because of diffusion across the chromium oxide layer because the area where the best nanotubes grow is also the one depleted of chromium and oxygen.

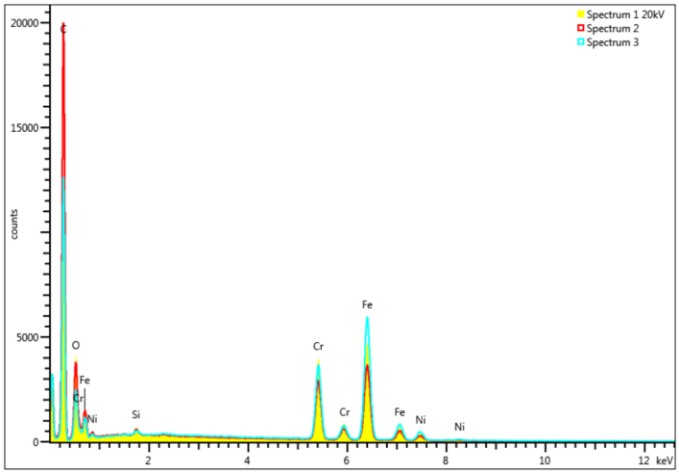

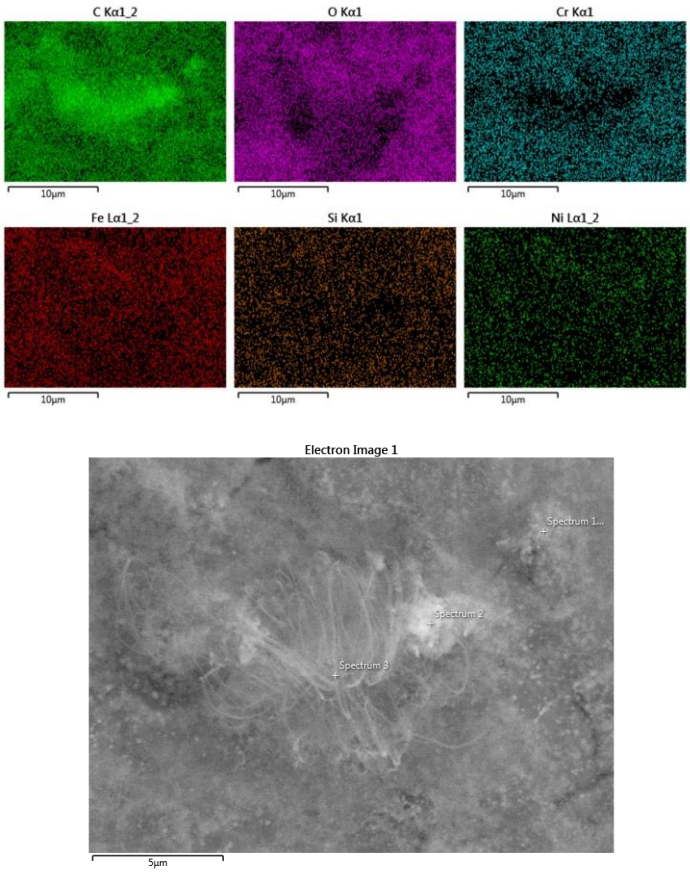

Figure 12

SEM-EDS results of the post-CVD 175 kHz 60 mm/s square. Peaks indicating the presence of six elements were detected; carbon, oxygen, iron, chromium, nickel, and silicon.

Discussion

The results of this study lent some credence to the initial hypothesis laid out in this study, but the answer is not completely decided. This hypothesis was that the term “dewetting cycles” is a misnomer and a simplification, and there is a benefit to decoupling scanning speed and frequency. To that end, it was shown that scanning speed has a dominant effect on fluence while frequency is the sole factor in pulse energy.

From the coloration of the stainless steel, it is generally the case that frequency, and therefore pulse energy affects what can be best described as the hue. This is determined through thin film interference by the thickness of the oxidation layer. This is not to say that fluence has no effect on the hue, but frequency and pulse energy dominate. The coloration effect of scanning speed and fluence is more in line with the saturation of the color of the surface. This is determined by the feature density. Combined, these knobs precisely control the surface structure and composition and can lead to wildly different outcomes for VA-CNT growth.

The SEM results were in line with what was found in the Dasbach study. Cauliflower structures occurred at what they referred to as high DCs, or at low scanning speeds. It should be noted that increasing frequency leads to less pulse energy, and therefore smaller oxide layers though it would increase the number of DCs. This is a large reason while decoupling frequency and scanning speed is important.

From the SEM-EDS, it was shown that the best VA-CNT growth occurs in chromium oxide depleted zones. This cannot be a result of the CNT growth blocking out the chromium oxide surface, because if that were the case, it would also decrease the amount of silicon, iron, and nickel in that area, which does not happen. Instead, this can be attributed to more iron and nickel diffusing across the chromium-rich layer to the surface, creating more ideal sites for VA-CNT growth.

There is much more work to be done in this area, as this study only scratches the surface. Further exploration of the parameter space using SEM and Raman spectroscopy is needed to identify the best frequencies and scanning speeds for VA-CNT growth. A related test that would be useful would be to study the extent to which dewetting occurs in a pulse laser on 304 stainless steel. This would help in determining whether DCs are a proper term to be used in this situation or a misnomer.

Several errors were present in this research. First, the samples were not as smooth and scratch free as would be desired. In the process of cutting them into disks, the protective adhesive had to be removed, exposing the samples to some minor scratches. This may have had an effect on the lack of uniformity across the squares. Another source of error was performing the CVD on the entire group of 42 squares at once. While this allowed for fast and easy comparison across the sample space, it added confounding variables. It is possible that the different locations influenced each other or depleted the ethylene carrier gas of carbon as it spread across a wide area.

Conclusion

In conclusion, the intersection of VA-CNT growth via CVD and pulsed laser oxidation of SS is complicated but has clear potential and applications. This study found reason to believe that the literature standard term of dewetting cycles may not be the best parameter by which to examine this process. Dewetting is likely not the driving factor in nanoparticle production, and scanning speed and frequency have differing effects on SS surface composition and therefore VA-CNT growth. Due to the short duration of this study, several potential sources of error were created along the way, including scratched samples and simultaneously running different trials in one CVD run. In future work, these can be addressed. Additionally, it is recommended to continue to explore the sample space, at higher and lower frequencies and scanning speeds. More characterization methods would also prove useful, such as Raman spectroscopy.

References

[1] Dasbach, M., Pyschik, M., Lehmann, V., Parey, K., Rhinow, D., Reinhardt, H. M., & Hampp, N. A. (2020). Assembling Carbon Nanotube Architectures. *ACS Nano*, *14*(7), 8181–8190. https://doi.org/10.1021/acsnano.0c01606

[2] Asghar, U., Qamar, M. A., Othman Hakami, Ali, S. K., Imran, M., Farhan, A., Parveen, H., & Sharma, M. (2024). Recent Advances in Carbon Nanotube Utilization in Perovskite Solar Cells: A Review. *Micromachines*, *15*(4), 529–529. https://doi.org/10.3390/mi15040529

[3] Kohls, A., Ditty, M. M., Fahimeh Dehghandehnavi, & Zheng, S.-Y. (2022). Vertically Aligned Carbon Nanotubes as a Unique Material for Biomedical Applications. *ACS Applied Materials & Interfaces*, *14*(5), 6287–6306. https://doi.org/10.1021/acsami.1c20423

[4] Pattinson, S. W., Viswanath, B., Zakharov, D. N., Li, J., Stach, E. A., & Hart, A. J. (2015). Mechanism and Enhanced Yield of Carbon Nanotube Growth on Stainless Steel by Oxygen-Induced Surface Reconstruction. *Chemistry of Materials*, *27*(3), 932–937. https://doi.org/10.1021/cm504209u

[5] Pawlitzek, F., Althues, H., Schumm, B., & Kaskel, S. (2017). Nanostructured Networks for Energy Storage: Vertically Aligned Carbon Nanotubes (VACNT) as Current Collectors for High-Power Li4Ti5O12(LTO)//LiMn2O4(LMO) Lithium-Ion Batteries. *Batteries*, *3*(4), 37. https://doi.org/10.3390/batteries3040037

[6] Reinhardt, H., Hellmann, C., Nürnberger, P., Kachel, S., & Hampp, N. (2017). Free Form Growth of Carbon Nanotube Microarchitectures on Stainless Steel Controlled via Laser-

Stimulated Catalyst Formation. *Advanced Materials Interfaces*, *4*(16). https://doi.org/10.1002/admi.201700508

[7] Roumeli, E., Diamantopoulou, M., Serra-Garcia, M., Johanns, P., Parcianello, G., & Daraio, C. (2019). Characterization of Vertically Aligned Carbon Nanotube Forests Grown on Stainless Steel Surfaces. *Nanomaterials*, *9*(3), 444. https://doi.org/10.3390/nano9030444

[8] Sano, N., Yamamoto, S., & Tamon, H. (2014). Cr as a key factor for direct synthesis of multi-walled carbon nanotubes on industrial alloys. *Chemical Engineering Journal*, *242*, 278–284. https://doi.org/10.1016/j.cej.2013.12.073

[9] Yahyazadeh, A., Nanda, S., & Dalai, A. K. (2024). Carbon Nanotubes: A Review of Synthesis Methods and Applications. *Reactions*, *5*(3), 429–451. https://doi.org/10.3390/reactions5030022

[10] Zhuo, C., Wang, X., Nowak, W., & Levendis, Y. A. (2014). Oxidative heat treatment of 316L stainless steel for effective catalytic growth of carbon nanotubes. *Applied Surface Science*, *313*, 227–236. https://doi.org/10.1016/j.apsusc.2014.05.189